ELSEVIER

Contents lists available at ScienceDirect

European Journal of Pharmaceutical Sciences

journal homepage: www.elsevier.com/locate/ejps





Engineered-affibody conjugates contribute to the specific targeting and cellular retention of polyplexes in Erbb3 overexpressed lung cancer cells

Siyu Chen ^{a,1,2}, Anny Nguyen ^{a,1}, Joschka T. Müller ^a, Müge Molbay ^a, Aditi Mehta ^a, Sahana Sheshachala ^b, Kemal Baskaya ^b, Nathan Adams ^b, Simone Pinto Carneiro ^a, Olivia M. Merkel ^{a,c,*}

- a Ludwig-Maximilians-University, Department of Pharmacy, Pharmaceutical Technology and Biopharmaceutics, Butenandtstraße 5-13, 81377 Munich, 81377, Germany
- ^b NanoTemper Technologies GmbH, Toelzer straße 1, 81379, Munich, Germany
- c Ludwig-Maximilians-Universität Munich, Member of the German Center for Lung Research (DZL), 81377, Munich, Germany

ARTICLE INFO

Keywords: mRNA deliveryl Polyplex KRAS mutant lung cancer Erbb3 receptor Tumor targeting Affibody

ABSTRACT

Ligand-modified nanoparticles have shown the ability to specifically bind to tumor cells, improving retention in tumors after initial accumulation driven by the enhanced permeability and retention effect. These particles are typically engineered to bind to receptors overexpressed in cancer cells compared to healthy cells, such as the HER3 (Erbb3) receptor in lung cancer. In this study, we confirmed the overexpression of Erbb3 in various KRAS mutant lung cancer cell lines. An engineered affibody, well-established in previous research, was selected to target Erbb3 as a proof of concept. The affibody was integrated into the particle system via two distinct strategies. In the pre-functionalization approach, the affibody was conjugated to PEI or C14-PEI using SPDP as a linker. A spectral shift technique was then used to assess the affinity of the affibody and affibody conjugates toward Erbb3, allowing us to estimate the half-maximal effective concentration (EC50). Following synthesis and characterization, various polyplex formulations were prepared, including mRNA complexes with PEI-affibody, C14-PEI/PEI-affibody, and C14-PEI/C14-PEI-affibody. In the post-functionalization approach, polyplex formulations composed of different blends of C14-PEI and functionalized Azido-PEI were initially prepared and subsequently modified with DBCO-functionalized affibody via click chemistry. These formulations were prepared at various nitrogen to phosphate (N/P) ratios and characterized in terms of particle size, polydispersity index (PDI), and zeta potential. We also evaluated cellular uptake and eGFP mRNA expression to understand how the different formulations and conjugates influenced ligand-modified polyplex properties and delivery behavior. Our results demonstrated that affibody conjugates can specifically target Erbb3 and promote polyplex accumulation in KRAS-mutated lung cancer cells. We further analyzed the impact of conjugation methods and affibody density on polyplex design and performance. In conclusion, this study highlights the advantages of using specific targeting ligands. By optimizing formulation components, conjugation methods, and ligand density, various targeting ligands can be attached to polyplexes, enhancing cell-specific targeting, internalization, and retention. These findings provide valuable insights and a foundation for future targeted therapies and polyplex design.

1. Introduction

Lung cancer is a malignant tumor that originates in the lung. According to the Global Cancer Statistics 2022, it remains the most commonly diagnosed cancer and the leading cause of cancer-related deaths. (Bray et al., 2024) The disease typically arises from genetic

damage to the DNA of airway cells, often linked to cigarette smoking or inhalation of harmful chemicals. (Leiter et al., 2023) Lung cancer is also influenced by geography, ethnicity, gender, and socioeconomic factors. As a heterogeneous disease, it encompasses different subtypes, each requiring tailored treatments. (de Sousa and Carvalho, 2018) In addition to traditional methods such as surgery, radiotherapy, and

^{*} Corresponding author at: Ludwig-Maximilians-University, Department of Pharmacy, Munich, 81377 Germany. E-mail address: olivia.merkel@lmu.de (O.M. Merkel).

¹ These authors contributed equally.

² Current address: Key Laboratory of Marine Genetic Resources, Third Institute of Oceanography, Ministry of Natural Resources, Xiamen, Fujian, 361005, China.

chemotherapy, targeted therapies and immunotherapies have been introduced in clinical settings. (Barr et al., 2024) However, survival rates remain low, especially in metastatic cases, with challenges such as drug resistance and systemic toxicity still persisting.

Nanomedicine, a rapidly growing field, offers promising solutions to these biological challenges. Numerous nanoparticle-based therapies have been studied to treat cancer, (Li et al., 2024) neurodegenerative diseases, (Helmschrodt et al., 2017) and infections. (Ryan et al., 2021) Nanoparticles (NPs), due to their unique properties, present new opportunities for targeted lung cancer therapy. (Woodman et al., 2021) As drug carriers, NPs enhance targeting accuracy, drug stability, and increase drug accumulation in tumor tissues, leading to improved anti-tumor effects. (Liu et al., 2023) Various forms of NPs have been explored, including lipid nanoparticles (LNPs), (Jurgens et al., 2024) polyplexes, (Jin et al., 2024) gold NPs, (Lee et al., 2017) endosomal vesicles, (Jang et al., 2013) and peptide NPs. (Ramakrishna et al., 2014) The success of mRNA vaccines for COVID-19 has further propelled the field of mRNA therapeutics, establishing it as a viable treatment option in modern medicine. (Lokras et al., 2024) In our previous study (Chen et al., 2025), we described a cationic polymer, C14-PEI, which demonstrated low toxicity and effective mRNA delivery to lung cancer cells.

Recent studies have shown that targeted nanoparticles can specifically bind to tumor cells, enhancing their retention within tumors following initial accumulation due to the enhanced permeability and retention (EPR) effect. (Valcourt et al., 2018) The EPR effect refers to a universal pathophysiological phenomenon and mechanism in which macromolecular compounds such as albumin ligand-conjugated drugs beyond certain sizes (typically liposomes, nanoparticles, and macromolecular drugs) can progressively accumulate in the tumor vascularized area and thus achieve targeting delivery and retention of anticancer compounds into solid tumor tissue. (He et al., 2022) Due to the lack of effective lymphatic drainage in tumor tissue, the synergistic effect of multiple growth factors and inflammatory factors (such as vascular endothelial growth factor, VEGF) leads to abnormal transport of macromolecular drugs in tumor tissue, thus causing the EPR effect. (Wu, 2021) The efficiency of the EPR effect can be enhanced by modifying the surface of NPs to optimize their size and surface charge. In particular, improving the NPs' affinity for tumor cells can lead to better targeting and accumulation within the tumor microenvironment, resulting in more effective therapeutic delivery. Designing NPs to target specific receptors may enhance retention in the tumor region and reduce off-target effects, a strategy that shows significant potential for future clinical applications. While well-known receptors such as EGFR have been extensively studied, (Wang et al., 2017) novel overexpressed receptors provide attractive targets for new nanotherapeutics. For instance, Gabold et al. recently transferrin-modified chitosan nanoparticles for nose-to-brain delivery, demonstrating increased cellular uptake and faster passage through epithelial layers in glioblastoma models. (Gabold et al., 2023)

One receptor gaining attention in cancer research is receptor tyrosine-protein kinase Erbb3, also known as HER3 (human epidermal growth factor receptor 3), which plays a key role in tumor progression and resistance to treatment. (Mishra et al., 2018) Erbb3, a member of the type I RTK ERBB receptor family, shares a common structure with other ERBB receptors. It consists of an extracellular binding domain (ECD), an intracellular tyrosine kinase domain, and a C-terminal tail. The ECD is divided into four domains: domains I and III have β-helical structures that contain ligand-binding sites, while domains II and IV consist of seven small disulfide-containing modules forming a β -hairpin loop, facilitating interaction between domains II and IV. (Cho and Leahy, 2002) Although the tyrosine kinase domain of Erbb3 is inactive, it forms active heterodimers with other members of the ErbB family. One of the most potent tumorigenic heterodimers is the HER2/HER3 pair, which activates key signaling pathways such as PI-3K/Akt and MAPK/MEK4. (Mishra et al., 2018; Sithanandam and Anderson, 2008) Increased expression of Erbb3 is linked to various cancers, (Tanner et al., 2006;

Lipton et al., 2013; Kumagai et al., 2018; Beji et al., 2012; Qian et al., 2015) including lung cancer, where its expression is notably higher in stage IA1 lung adenocarcinoma, particularly in cases without EGFR mutations. (Kumagai et al., 2018) Studies have shown that elevated Erbb3 levels are also associated with poor chemotherapy outcomes in both lung and breast cancers. (Sithanandam and Anderson, 2008) A promising therapeutic approach involves an engineered affibody targeting Erbb3, as reported by Schardt and colleagues. (Schardt et al., 2017) This affibody specifically binds to Erbb3 without triggering downstream signaling, making it a valuable ligand for conjugation with polyplexes in targeting lung cancer cells.

This study aimed to investigate affibody conjugation using PEI and C14-PEI while exploring two functionalization strategies: preconjugation (polymer functionalized before polyplex formation) and post-conjugation (affibody added after polyplex assembly). It further evaluates the interaction between self-assembled nanoparticles decorated with an engineered affibody and overexpressed Erbb3 in KRAS mutant lung cancer cells. After confirmation of the overexpression of Erbb3 in KRAS-mutant lung cancer cells, we employed the engineered affibody as a proof-of-concept targeting ligand due to its wellcharacterized ability to bind the Erbb3 receptor. The spectral shift test was performed to explore the affinity and receptor binding behavior of affibody and polymer conjugates. Polyplexes were prepared based on the formulation parameters, chosen conjugation strategy, and affibody density. Their characteristics were assessed in terms of particle size, polydispersity index (PDI), zeta potential, cellular uptake, and gene expression in three different Erbb3 expressing cell lines.

2. Materials & methods

2.1. Materials

4-(2-hydroxyethyl)-1-piperazineethanesul-fonic acid (HEPES), Dulbecco's Phosphate Buffered Saline (PBS), 0.05 % trypsin-EDTA, RPMI-1640, fetal bovine serum (FBS), bovine serum albumin (BSA), 1,2-epoxytetradecane, branched PEI 600 Da, Tris-buffered saline, Tween 20, Penicillin-Streptomycin solution, FluorSave Reagent, Lysogeny broth (LB), ampicillin, 6-diamidino-2-phenylindole dihydrochloride (DAPI), Brilliant Blue, sodium dihydrogenphosphat, isopropyl β -D-1-thiogalactopyranoside (IPTG), 2,4, 6-trinitrobenzene sulfonic acid (TNBS), sodium azide, paraformaldehyde (PFA), sodium chloride, imidazole, lysozyme, Benzonase® Nuclease and Accutase® solution were purchased from Sigma-Aldrich (Darmstadt, Germany). Dulbecco's Modified Eagle Medium (DMEM), LipofectamineTM 2000, PierceTM BCA Protein Assay kit, Phusion Site-Directed Mutagenesis Kit, trypan blue, Novex™ WedgeWell™ 8–16 % Tris-Glycin gel, Rhodamine-Phalloidin, AF488conjugated goat anti-rabbit IgG (H+L) secondary antibody, HisPurTM Ni-NTA Spin Purification Kit, FITC Labeling Kit, Pierce Universal Nuclease, dithiothreitol (DTT), Succinimidyl 3-(2-pyridyldithio)propionate (SPDP), and PEG12-SPDP were bought from Thermo Fisher Scientific (Planegg, Germany). Azido-PEG4-NHS-ester (MedChemexpress, Sollentuna, Sweden), AF647 labeled eGFP mRNA (RiboPro, Netherlands), Dibenzocyclooctyne (DBCO)-PEG12-NHS-ester (Hycultec, Beutelsbach, Germany), PEI 5 kDa (Lupasol G100, BASF, Germany), eGFP mRNA (RiboPro, Netherlands), PE-labeled anti-Erbb3 antibody (Biolegend, USA), PE Mouse IgG2a κ Isotype Control (Biolegend, USA), primary antibodies for Erbb3 (Cell Signaling Technology, MA, USA), Her3 (Erbb3, Sino biological, China), protein Labeling Kit RED-NHS 2_{nd} Generation (NanoTemper Technologies GmbH, Munich, Germany), Escherichia coli strain BL21 (New England Biolabs, Frankfurt am Main, Germany), and Vivaspin 6 centrifugal concentrator (Sartorius, Germany) were purchased from the suppliers indicated. Cy5-mRNA, AF405mRNA, Cy5-Her3, engineered trivalent affibody against Erbb3, and FITC-affibody were prepared and labeled in the laboratory. Methanol, ethanol, acetic acid, and acetone were provided by Ludwig-Maximilians-University Munich.

2.2. Cell culture

A549, Hop-62, H358, and H358M cells were cultured in RPMI-1640 medium, while 16HBE14o- cells were grown in DMEM. Both media were supplemented with 10 % heat-inactivated FBS and 1 % penicillinstreptomycin. The cells were subcultured and maintained in a humidified incubator at 37 $^{\circ}$ C with 5 % CO₂.

2.3. Erbb3 receptor expression

UCSC Xena was used to cross-analyze clinical data from The Cancer Genome Atlas Program (TCGA) and The Genotype-Tissue Expression (GTEx) project to confirm Erbb3 expression in lung cancer patients. (Goldman et al., 2020) To assess Erbb3 surface accessibility and density, flow cytometry (FACS) and immunofluorescence tests were performed on healthy lung cells (16HBE140-, WT KRAS) and lung cancer cells (A549, KRAS G12S; Hop62, KRAS G12C).

For the FACS analysis, cells were cultured 24 h prior to staining. After washing with PBS and detaching with 0.05 % trypsin-EDTA, cells were resuspended to approximately 1×10^6 cells/mL in cold PBS with 3 % BSA and 1 % sodium azide. Each sample was incubated with either PE-labeled anti-Erbb3 antibody or PE Mouse IgG2a κ Isotype Control (Biolegend, USA) at 4 $^\circ$ C in the dark for 30 min. Cells were washed three times by centrifugation at 500 xg for 5 min, then resuspended in cold PBS with 3 % BSA and 1 % sodium azide for FACS analysis.

For immunofluorescence with confocal imaging, cells were seeded on coverslips in a 24-well plate and incubated for 24 h. After washing with PBS, cells were fixed with 4 % PFA for 15 min and permeabilized with PBS containing 0.3 % Tween-20 for 10 min. Blocking was done with 5 % BSA in TBST for 1 h. Primary anti-Erbb3 antibody (Cell signaling, USA) was incubated with the cells at 4 °C overnight, followed by incubation with an AF488-conjugated secondary antibody (Thermo Fisher, USA) for 1 h at room temperature in the dark. After staining Factin with Rhodamine-Phalloidin (Thermo Fisher, USA) and the nucleus with DAPI (Sigma-Aldrich, Germany), the coverslips were mounted on slides using FluorSave Reagent (Sigma-Aldrich, Germany). Confocal images were captured using the blue channel (350/470 nm) for DAPI, the green channel (490/517 nm) for AF488, and the red-orange channel (540/565 nm) for Rhodamine-Phalloidin on a confocal microscopy (Leica SP8 inverted, software: LAS X, Leica Microsystems GmbH, Germany).

2.4. Affibody expression

The original pET45b-affibody constructs were a kind gift from Dr. Steven M. Jay at the University of Maryland. (Schardt et al., 2017) To introduce a cysteine residue to enable conjugation, site-directed mutagenesis was performed using a PCR-based approach followed by DpnI digestion to eliminate the template plasmid as per the description from the Phusion Site-Directed Mutagenesis Kit (Thermo Fisher, USA). Next, the plasmids were transformed into *E. coli* strain BL21 (New England Biolabs) using the heat shock method. (Froger and Hall, 2007) Subsequently, single colonies were grown overnight in 10 mL of LB broth with 100 µg/mL ampicillin inoculated from a 3 mL overnight starter culture, incubated at 37 °C, shaking. To generate glycerol stocks, 500 µL of the overnight culture was added to 500 µL of 50 % glycerol in a 2 mL screw top cryotube and gently mixed, and stored at $-80\,^{\circ}\text{C}$.

The *E. coli* BL21 strain containing Affibody-His-tag plasmids was cultured from glycerol stock in 5 mL of LB with 100 μ g/mL ampicillin at 37 °C, shaking at 110 rpm, until the culture became turbid. This bacterial culture was then transferred to 200 mL of LB media with 100 μ g/mL ampicillin and incubated overnight at 37 °C, shaking at 220 rpm, until the optical density (OD600) reached 0.4–0.8. Protein expression was induced by adding IPTG to a final concentration of 1 μ M, followed by incubation at 30 °C while shaking at 220 rpm for 4 h. The bacterial cell pellet was then collected by centrifugation at 4000 xg for 30 min.

Affibody extraction was carried out using the HisPurTM Ni-NTA Spin Purification Kit (Thermo Fisher, USA) according to the manufacturer's instructions with an adjustment. Generally, the bacterial pellet was resuspended in 1.4 mL of lysis buffer (50 mM NaH₂PO₄, 300 mM NaCl, 10 mM imidazole, pH 8.0) and treated with lysozyme (Sigma-Aldrich, Germany), Benzonase® Nuclease (Sigma-Aldrich, Germany), and Pierce Universal Nuclease (ThermoFisher, USA) to lyse the bacterial cells and remove nucleic acids, followed by 30 min of incubation on ice. The lysate was then applied to equilibrated HisPurTM Ni-NTA columns and allowed to bind to the resin at 4 °C for 30 min. After three washes with wash buffer (50 mM NaH₂PO₄, 300 mM NaCl, 20 mM imidazole, pH 8.0), the affibody was eluted using elution buffer (50 mM NaH₂PO₄, 300 mM NaCl, 500 mM imidazole, pH 8.0) and stored at -80 °C in the presence of 5 mM DTT.

2.5. Affibody quantification and qualification

The concentration of the purified affibody was determined using a bicinchoninic acid (BCA) assay, and its purity and integrity were assessed via sodium dodecyl sulfate-polyacrylamide gel electrophoresis (SDS-PAGE). The Pierce™ BCA Protein Assay Kit (Thermo Fisher, USA) was performed according to the manufacturer's instructions. A BSA standard curve was prepared by diluting BSA in water across six concentrations, ranging from 2 mg/mL to 0.0625 mg/mL. The BCA working reagent was obtained by mixing 50 parts of reagent A with 1 part of reagent B. For the assay, 20 µL of each BSA dilution or sample was combined with 200 µL of BCA working reagent in a 96-well plate and incubated at 37 °C for 30 min, protected from light. Absorbance at 562 nm was measured using a Tecan plate reader, with the blank standard absorbance subtracted from all other values. For SDS-PAGE, equal amounts of protein were loaded onto an 8-16 % Tris-Glycine gel (NovexTM WedgeWellTM), and electrophoresis was run at 100 V for 1 h in the running buffer. The gel was stained with Brilliant Blue (Sigma-Aldrich, Germany) for 1 h at room temperature, followed by destaining with water and destaining buffer (10 % acetic acid, 50 % methanol, and 40 % H₂O). Protein bands were visualized immediately using a ChemiDoc imaging system (BioRad, USA).

2.6. Affibody binding analysis

To assess the Erbb3-specific binding of the affibody, it was labeled with fluorescein isothiocyanate (FITC) using the FITC Labeling Kit (Thermo Fisher, USA). The purified affibody was incubated with FITC solution overnight at 4 $^{\circ}$ C, protected from light. After incubation, the labeled affibody was recovered using a Vivaspin 6 centrifugal concentrator (Sartorius, Germany) with a molecular weight cut-off (MWCO) of 10 kDa. The FITC-labeled affibody was then incubated with cells, as described in Section 2.3, to evaluate its binding affinity to Erbb3 via FACS.

2.7. Affibody conjugation and polyplex preparation

The affibody was incorporated into the particle system through two distinct functionalization methods. In the pre-functionalization strategy, PEI-affibody conjugates were prepared using an SPDP linker, followed by purification via ultrafiltration and ÄKTA chromatography as previously reported. (Kandil et al., 2020) Briefly, SPDP was added to 1 mL of 1 mg/mL 5 kDa PEI, stirred, and incubated overnight at room temperature. Simultaneously, since there is no endogenous cysteine in affibodies (Stahl et al., 2017), the SPDP was used to functionalize the affibodies site-specifically to enable conjugation (Figure S1). With the treatment of SPDP, disulfide bonds were introduced to the affibodies. Next, under nitrogen gas, DTT was used to reduce the disulfide bond in the affibody-SPDP conjugate and expose a sulfhydryl group for conjugation. After purification, pyridyldithiol-activated PEI and sulfhydryl-activated affibodies were mixed and stirred at 4 °C overnight.

The final conjugates were purified using ultrafiltration and ÄKTA at 280 nm chromatography, and the concentration of PEI was determined spectrophotometrically at 405 nm using a TNBS assay. For C14-PEI-affibody conjugates, a similar process was followed to couple affibodies with PEI, but PEG12-SPDP was used to modify the C14-PEI. Following conjugation, 1,2-epoxytetradecane was added to the solution for a ring opening reaction at 95 °C in absolute ethanol for 72 h while stirring. (Chen et al., 2025)

Polyplexes were prepared by combining PEI or PEI-affibody conjugate with RNA through electrostatic interactions. Specifically, 500 ng of eGFP mRNA and a predetermined amount of polymer or conjugate, based on the desired N/P ratios (nitrogen to phosphate ratio), were dissolved in high-purity water and mixed by pipetting and vortexing in $100~\mu L$ of 10~mM HEPES buffer, pH 7.4. The mixture was incubated at room temperature for 1~h.

For postmodified C14-PEI/PEI, blended-affibody conjugates, strainpromoted azide-alkyne cycloaddition (SPAAC) was employed to couple the affibody to PEI after polyplex formation.

C14-PEI was synthesized by adding 1,2-epoxytetradecane to a 1 mL solution of 600 Da branched PEI (100 mg/mL) at a 1:1 ratio of epoxy groups to primary amines, followed by a ring-opening reaction at 95 °C in absolute ethanol for 72 h under continuous stirring. The product was subsequently purified by dialysis in absolute ethanol for 48 h using the Pur-A-LyzerTM Midi Dialysis Kit with a 1000 Da molecular weight cut-off (Sigma-Aldrich, Germany).

For azido functionalization of 5 kDa PEI, a 1.5-fold molar excess of Azido-PEG4-NHS-ester was added to a 1~mg/mL PEI solution and stirred for 1~hour at room temperature. The modified PEI was then purified via ultracentrifugation using spin columns (Vivaspin 6, Sartorius, Germany) with 3~kDa molecular weight cutoff).

The affibody was functionalized with DBCO attached to a PEG12 spacer through NHS ester coupling. The incorporation of DBCO was quantified using spectrophotometric analysis by determining the ratio of absorbance at 280 nm to 309 nm (A280/A309).

C14-PEI and Azido-PEI were blended in various ratios, and polyplexes were prepared as previously described in 10 mM HEPES buffer at pH 7.4. Following 1 hour of incubation, nanoparticles were reacted with Affibody-DBCO at a molar ratio of 1:10 (DBCO to Azides) and incubated for 2 h at room temperature.

2.8. Particle characterization

Polyplex characterization was performed using a Zetasizer Ultra (Malvern, UK). To measure the hydrodynamic diameter, polydispersity index (PDI), and zeta potential, 100 μL of each polyplex sample in 10 mM HEPES buffer, pH 7.4, was placed in a disposable micro-cuvette (Malvern, UK). The hydrodynamic diameter and PDI were determined by measuring at a 173° backscatter angle with 15 runs per sample, and measurements were repeated three times. For zeta potential measurements, the polyplexes were diluted with 700 μL of HEPES buffer and transferred to a folded capillary cell (Malvern, UK). Three measurements were taken for each sample using the same device.

2.9. Polyplex transfection

To evaluate the delivery efficiency of mRNA by polyplexes, we assessed the cellular uptake of fluorescently labeled mRNA (AF405-mRNA, Cy5-mRNA or AF647-mRNA) and the expression of the enhanced green fluorescent protein (eGFP) reporter gene using flow cytometry.

Hop62 cells were used for testing PEI-affibody polyplexes, while A549, Hop62, and H358 cells were used for both pre- and post-functionalized C14-PEI/PEI-affibody and C14-PEI/C14-PEI-affibody polyplexes.

For pre-functionalized polyplexes, 30,000 cells per well were seeded in 24-well plates with 500 μL of growth medium and transfected with

500 ng of mRNA.

For post-modified polyplex screening, 10,000 cells per well were plated in 96-well plates with 200 μL of medium, using an adjusted mRNA dose of 200 ng per well. After 24 h of incubation at 37 $^{\circ} C$ with 5 $^{\circ} CO_2$, the cells were transfected with formulations encapsulating eGFP-mRNA and fluorescent-labeled mRNA. Following another 24 h of transfection, cells were washed with PBS and detached using 0.05 $^{\circ} L$ trypsin-EDTA. The detached cells were collected in 1.5 mL Eppendorf tubes, centrifuged at 500 x g for 5 min, and the supernatant was removed. Cells were washed with PBS and centrifuged again. The final cell pellet was resuspended in fresh PBS, and fluorescence intensity was measured using the Attune NxT flow cytometer (Thermo Fisher, Germany).

2.10. Labelling of HER3 for spectral shift analysis

HER3 (Erbb3, Sino biological, China) was labeled with Protein Labeling Kit RED-NHS 2_{nd} Generation (cat# MO-L011, NanoTemper Technologies GmbH, Germany). The labeling kit is specifically designed for RED detectors in Monolith X. In particular, 10 μM of HER3 (40 $\mu L)$ was incubated with 3x molar excess of RED-NHS 2_{nd} Generation dye (10 $\mu L)$ in NHS buffer. After 1 h of incubation in the dark, the labeled protein was purified using B-column of the labeling kit. Protein concentration (971 nM) and degree of labeling (0.45) were determined using Nanodrop.

Ligand samples were prepared using a 16 or 24-point serial dilution in HEPES buffer (pH 7.4) with 10 μL in each PCR tube. 10 μL of the target (RED-NHS labeled HER3) were added to each ligand sample. 10 μL of the complex were loaded into premium coated capillaries (NanoTemper Technologies GmbH, Germany), and into the Monolith X. All Binding affinity measurements were conducted using the Monolith X instrument (NanoTemper Technologies GmbH, Germany), which is equipped with dual-emission detection optics. Fluorescence was recorded at 650 nm and 670 nm simultaneously for 5 s for each ratiometric reading. The data was processed using MO. Control software (NanoTemper Technologies GmbH, Germany), and the results were used to calculate the half maximal effective concentration (EC50).

2.11. Statistics

All results are given as mean value \pm standard deviation (SD) of triplicate experiments (n=3) unless stated otherwise. Statistical significance was investigated using one-way ANOVA or two-way ANOVA. All statistical analyses were performed using GraphPad Prism software (GraphPad Software, USA).

3. Results and discussion

$3.1.\ Erbb3$ over-expressed in KRAS mutated lung cancer cells

TCGA and GTEx databases were used to confirm Erbb3 expression in lung cancer patients (Fig. 1A). The data set includes 830 lung adenocarcinoma (LUAD) samples, with 483 tumor tissues and 347 normal tissues. The expression of Erbb3 was presented as Log2 TPM (transcripts per million) + 1. Statistical analysis revealed that Erbb3 is significantly upregulated in tumor tissues compared to normal tissues.

Although previous studies have demonstrated Erbb3 overexpression in lung cancer cells, variables such as handling, passage number, and cell line source can influence cellular characteristics. (Witta et al., 2009; Wadajkar et al., 2017) Therefore, Erbb3 expression was examined and compared between healthy lung epithelial cells (16HBE140-) and lung cancer cell lines (A549, H358M and Hop62) using flow cytometry and confocal microscopy. Cells were incubated with labeled Erbb3 antibodies, and median fluorescence intensity (MFI) was measured through flow cytometry, followed by confocal microscopy imaging. For flow cytometry (FACS), 16HBE140- (KRAS WT), A549 (KRAS G12S), Hop62 (KRAS G12C), and H358M (KRAS G12D) cells were used. Cells were

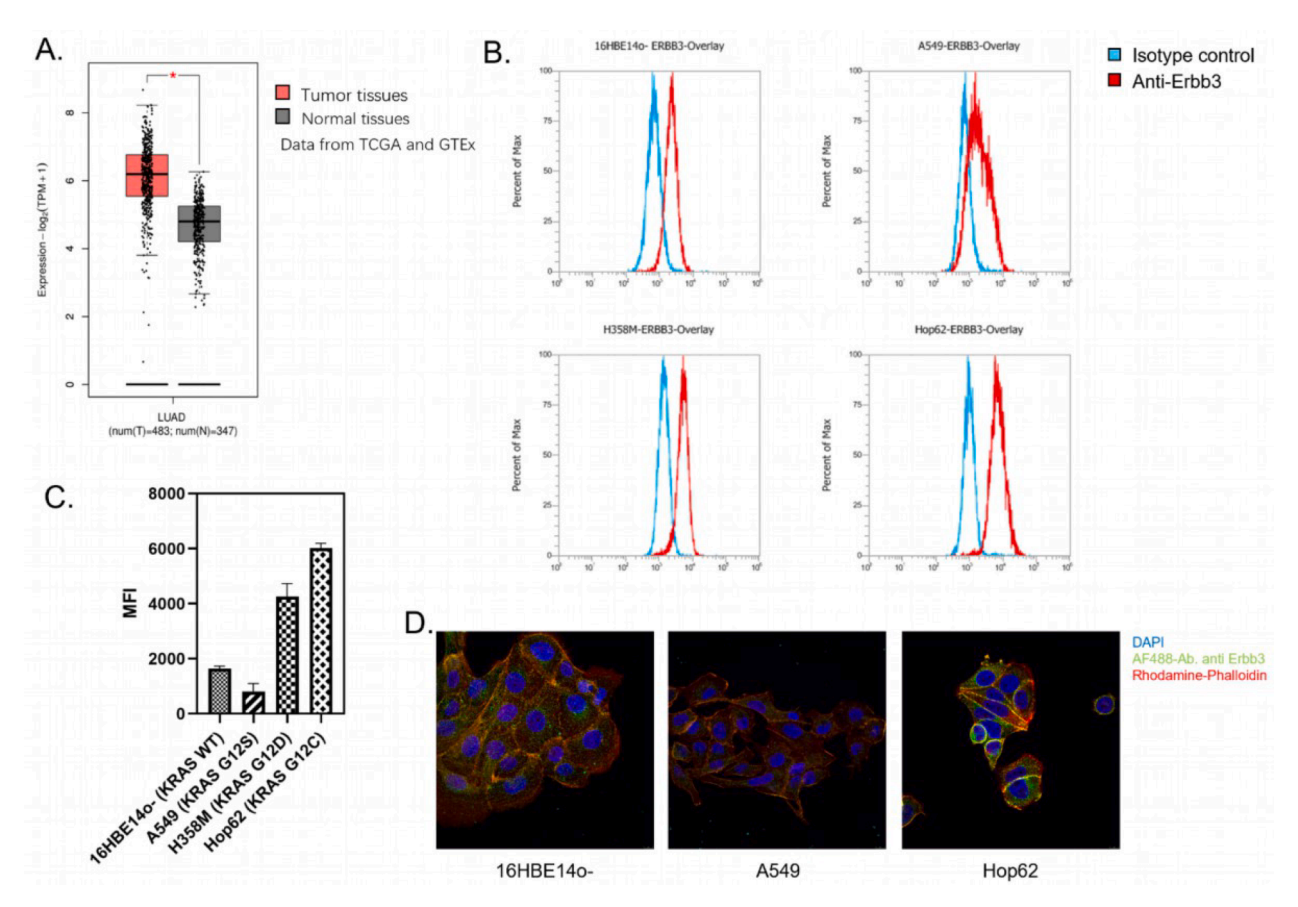


Fig. 1. The expression of Erbb3 in lung cancer. A) Expression of Erbb3 in lung adenocarcinoma patients; B) Levels of Erbb3 receptors in lung cells measured by FACS; C) MFI of FACS measurement in lung cells; D) Erbb3 expression in lung cells assessed by confocal microscopy.

co-incubated with PE-conjugated anti-Erbb3 antibodies for 30 min prior to measurements, and isotype antibodies served as negative controls. The data demonstrated that Hop62 and H358M cells exhibited significant Erbb3 overexpression compared to 16HBE14o-, with a 3.67- and 2.39-fold increase, respectively (Fig. 1C). In contrast, A549 cells did not show a higher MFI than 16HBE14o-, although a shift in the positive signal was observed, consistent with previous studies (Fig. 1B and 1C). (Witta et al., 2009; Coldren et al., 2006)

These findings were corroborated by the confocal microscopy images (Fig. 1D). The images show blue-stained nuclei (DAPI), red-stained F-actin (Rhodamine-Phalloidin), and green dots representing Erbb3 receptors labeled with AF488-conjugated antibodies. In 16HBE140- cells (KRAS WT), Erbb3 was distributed evenly on the cell surface and within the cytoplasm after internalization. However, in A549 cells, only a few green dots were detected, indicating lower Erbb3 expression. In Hop62 cells, a higher number of Erbb3 signals were observed, particularly on the cell surface. As a result, Hop62 cells were selected for subsequent transfection experiments, with A549 cells used as controls.

3.2. Extraction of engineered-affibody

Schardt and colleagues engineered a trivalent affibody (Schardt et al., 2017) utilizing the Z05413 affibody (Kronqvist et al., 2011) as the HER3 binding domain, connected with a flexible, protease-resistant peptide spacer (Jay et al., 2011) as a linker. As described above, we successfully constructed a plasmid encoding the affibody with His-tags in our lab and transformed it into *E. coli* BL21 strains. To isolate the affibody, bacteria were cultured in LB medium at 37 °C until the OD600 reached 0.4–0.8. Protein expression was induced for 4 h, and the purification was carried out using a HisPurTM Ni-NTA Spin Purification Kit. The purified affibody products were verified by SDS-PAGE (Fig. 2). In

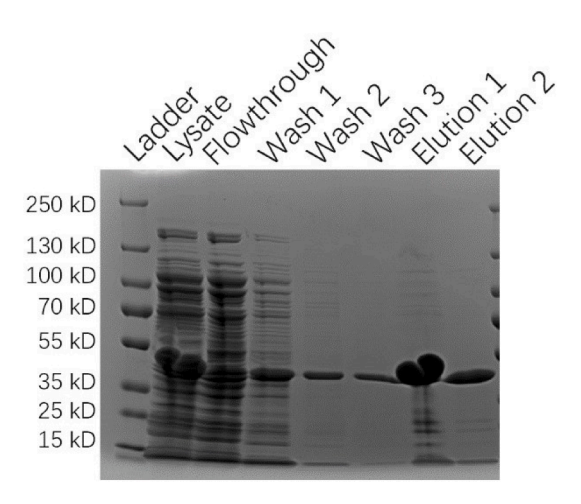


Fig. 2. SDS-PAGE showing the products from the affibdoy extraction.

the lysate and flowthrough (lanes 2 and 3), total bacterial proteins were detected. After washing (lanes 4–6), affibody products were clearly present in the elutes (lanes 7 and 8). The main protein bands were observed between 35–55 kDa, which is higher than the expected molecular weight of 30.5 kDa. This discrepancy is consistent with observations by Schardt et al., attributing the higher apparent molecular weight to electrophoretic interference from the affibody's helix-loop-helix motifs. (Schardt et al., 2017)

3.3. Prediction of the affibody's structure

To understand the properties of the affibody, we predicted its crystal structure with AlphaFold3. (Abramson et al., 2024) As shown in the ribbon diagram (Fig. 3A), the structure reveals a protein chain with a defined tertiary structure, featuring three distinct domains arranged side by side from the N-terminus to C-terminus. These domains appear as compact, likely globular regions, typical of binding domains, with surface features such as grooves or pockets that might interact with ligands or other proteins. The two regions between the binding domains, which are less structured or more elongated, represent the linkers. These linkers likely provide flexibility, allowing movement between the binding domains.

Then AlphaFold3 was used to predict the interaction between affibody and Erbb3. The structure of Erbb3, consisting of four domains, is shown in Fig. 3B, which aligns with the previous report from Cho and Leahy (Cho and Leahy, 2002). Fig. 3C shows the binding interaction between the affibody and Erbb3. The binding site is clearly visible, with the affibody's binding domains contacting domain I of Erbb3. This interaction region is likely crucial for the biological function of the complex, possibly involving key residues from both proteins. The binding appears to be complementary, with the surfaces of both proteins fitting together, suggesting a specific interaction driven by the shape and charge compatibility of the binding surfaces. The proteins are oriented in a way that likely reflects their natural binding conformation. While the linkers might allow some flexibility, the overall orientation is stable, suggesting a strong interaction.

3.4. Affinity between the affibody and Erbb3

Based on the AlphaFold3 prediction, a strong interaction between the affibody and Erbb3 was expected. To experimentally verify this interaction, the affibody was labeled with FITC and co-incubated with Hop62 cells at 37 $^{\circ}$ C for 24 h. Following incubation, FACS was used to measure fluorescence intensity (Fig. 4A). Trypan blue was applied to quench the fluorescence from any extracellular dye on the cell surface. Compared to the PBS-treated control group, the affibody-treated group exhibited a continuous increase in MFI over time, reaching a peak value of approximately 10,000 after 24 h. These results demonstrate that the affibody can interact with cell membranes and be internalized through receptor-mediated endocytosis.

A549 and Hop62 are both lung cancer cell lines, but A549 cells express much lower levels of Erbb3 than Hop62 cells. To further confirm the specificity of the affibody for Erbb3, FITC-labeled affibody was incubated with both cell lines. As shown in Fig. 4B, both A549 and Hop62 cells displayed similar fluorescence levels in the PBS-treated control group. However, after 24 h of affibody treatment, Hop62 cells exhibited significantly higher uptake of the labeled affibody compared to A549 cells. This result supports the conclusion that the affibody specifically recognizes and binds to Erbb3 receptors on Hop62 cells.

3.5. Pre-functionalization: C14-PEI-affibody conjugation

While the affibody was successfully shown to specifically target Erbb3-overexpressing lung cancer cells (Hop62 with KRAS G12S), the effects of Affibody-PEI conjugates were less clear (Figure S5). To overcome the challenges of mRNA delivery with PEI, a lipid-modified PEI (C14-PEI) was integrated into the polyplex system to introduce hydrophobic groups, promoting micelleplex formation and strengthening interactions with cell membranes. This approach, as demonstrated in our previous publication with A549 lung cancer cells, improved mRNA delivery and expression. (Chen et al., 2025) To further explore the potential of affibody-coupled polyplexes, we prepared conjugates of affibody and C14-PEI. The key difference between C14-PEI and PEI conjugation lies in the fact that the primary amine groups in C14-PEI are occupied by C14 alkyl chains, which may reduce the efficiency of

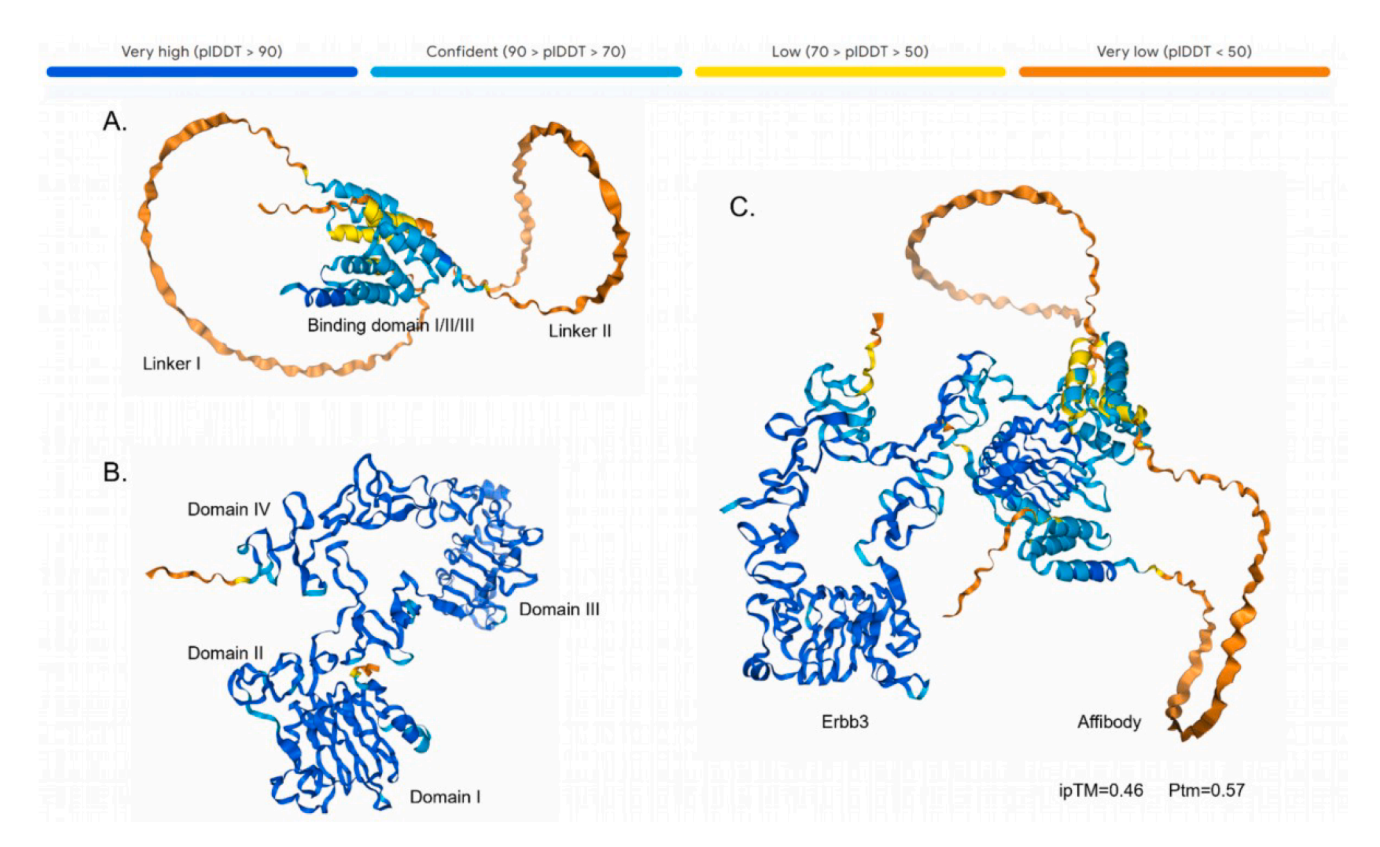


Fig. 3. Prediction of affibody structure and its binding with Erbb3 using AlphaFold3. A) Predicted structure of the affibody; B) Predicted structure of Erbb3; C) The predicted binding interaction between affibody and Erbb3.

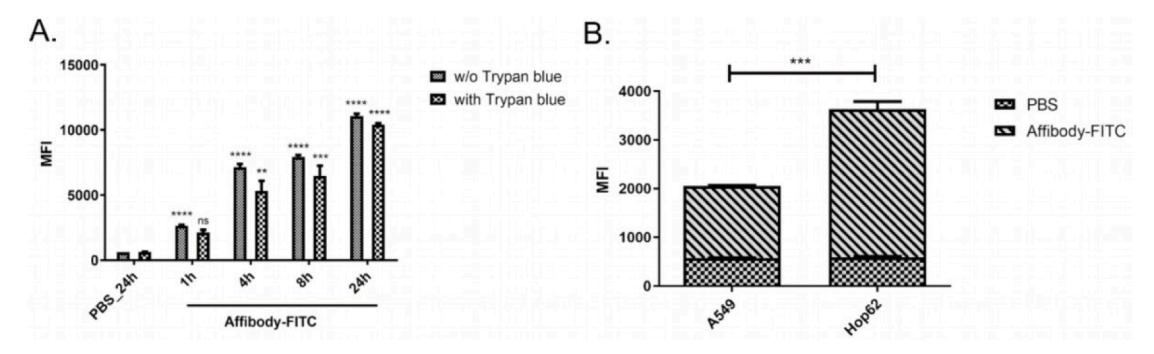


Fig. 4. Erbb3 mediates affibody cellular uptake. A) FITC labeled affibody uptake in Hop62 cells after 24 h (n = 3, ** $P \le 0.0021$, **** $P \le 0.0002$, **** $P \le 0.0001$); B) Comparison of specific binding of affibody in A549 and Hop62 cells 24 h after treatment with the labeled affibody (n = 3, t-test, *** $P \le 0.0001$).

affibody modification. To generate C14-PEI-affibody conjugates, PEI was first conjugated with affibodies using PEG12-SPDP as a linker, followed by coupling with C14 via a ring-opening reaction as previous description. Following preparation, the conjugates were purified using ultra-filtration and ÄKTA to remove any unbound compounds and free affibodies (Figure S6). PEG12-SPDP, in addition to providing NHS ester and pyridyldithiol reactive groups like SPDP, contains a 12-unit polyethylene glycol (PEG) spacer, offering a linker arm extending up to 54.1 Å The inclusion of PEG enhances solubility, increases linker length, and provides colloidal stability and biocompatibility to the particles. Additionally, PEGylation helps extend circulation time in vivo and reduces unwanted immune responses. (D'Souza and Shegokar, 2016; Johnston

et al., 2023)

3.6. Binding studies using spectral shift

Spectral shift technology was used to investigate the binding interaction of affibody and its conjugates with labeled HER3 (Langer et al., 2022) (RED-NHS $2_{\rm nd}$ Generation dye) using Monolith X (Nanotemper Technologies GmBH). This fluorescence-based biophysical technique is used to analyze molecular interactions by detecting wavelength shifts in the emission spectrum of a fluorophore attached to a target molecule upon ligand binding. When binding occurs, the chemical environment around the fluorophore changes, causing a shift in its emission

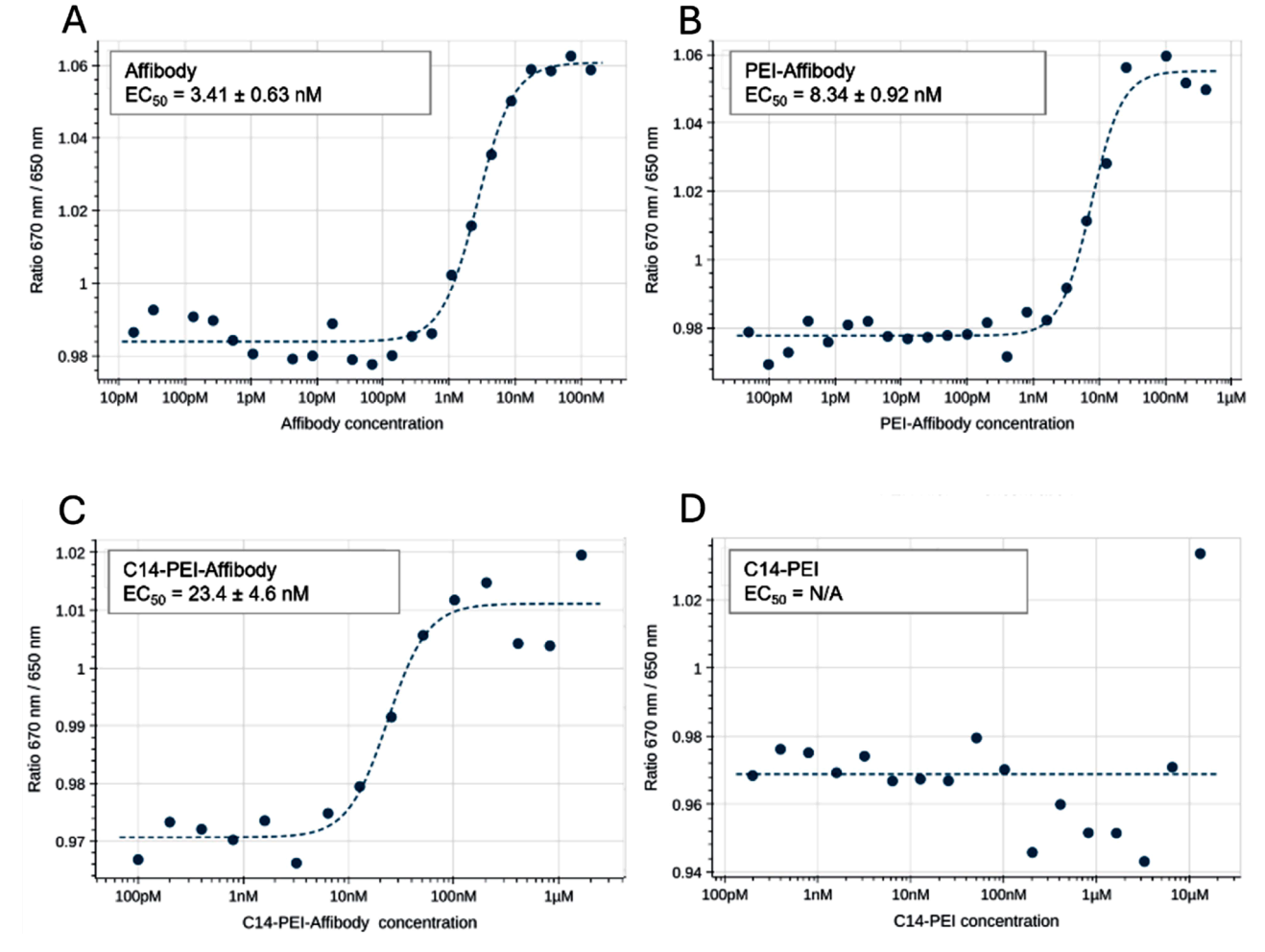


Fig. 5. Spectral shift dose-response curves for affibody (A), PEI-affibody conjugates (B), C14-PEI-affibody conjugates (C), and only C14-PEI (D).

wavelength. Here, the emission is detected at two distinct wavelengths (670 and 650 nm). The ratio of these intensities (670 nm/650 nm), known as spectral shift ratio, is used to obtain affinity parameters such as k_D (dissociation constant) and EC_{50} .

To determine the affinity with HER3, PEI-affibody conjugates and C14-PEI-affibody conjugates were used as ligands, while labeled HER3 functioned as target. Free affibody and C14-PEI served as positive and negative controls, respectively. The binding activity of the affibody and its conjugates with labeled HER3 is evaluated by deriving the EC50 from dose-response curves. A lower EC50 value indicates that less ligand is needed to achieve the response, suggesting a stronger apparent binding interaction. As shown in Fig. 5A, free affibody exhibited strong binding affinity, yielding an EC $_{50}$ of 3.41 \pm 0.63 nM. Both PEI-affibody and C14-PEI-affibody conjugates showed similar binding profiles (Figs. 5B and 5C), with measurable EC $_{50}$ at 8.34 \pm 0.92 nM and 23.4 \pm 4.6 nM, respectively, demonstrating that affibody conjugates retain function but with reduced affinity compared to free affibody. In contrast, within the same concentration range, C14-PEI did not exhibit any affinity for HER3 (Fig. 5D) until a very high concentration demonstrated unspecific binding.

3.7. Pre-functionalization: C14-PEI-affibody polyplex preparation

The density of proteins on nanoparticles significantly influences polyplex properties. Overcrowding of antibodies on the nanoparticle surface can create steric hindrance, reducing the ability of individual antibodies to bind effectively to their targets. (Yong et al., 2020) Additionally, excessive antibodies may alter the surface charge or stability of the nanoparticles, potentially affecting their performance in biological systems. (Guerrini et al., 2018) To optimize polyplex properties, a blending strategy was employed, wherein C14-PEI and C14-PEI-affibody were mixed in different proportions, with PEI-affibody used as a comparison. (Kandil et al., 2019) As described in Section 2.7, polyplexes were prepared by adding 0 %, 10 %, and 30 % C14-PEI-affibody or PEI-affibody conjugates to HEPES buffer containing C14-PEI. The polymer solution was vortexed and then incubated with the mRNA solution, allowing for self-assembly. As shown in Fig. 6, blending affibody conjugates led to increased particle size and reduced zeta potential across all formulations. This trend was particularly pronounced in the PEI-affibody blends. In the absence of affibody conjugates, C14-PEI polyplexes exhibited a size of approximately 300 nm and a zeta potential of around 40 mV, consistent with previous findings. (Chen et al., 2025) However, as the affibody proportion increased, notable changes were observed, which again can be explained by the negative charge of the affibody at pH 7.4. For instance, at 30 % affibody-conjugation, the C14-PEI/PEI-affibody polyplexes reached a size of 3000 nm with a zeta potential of 6 mV, while C14-PEI/C14-PEI-affibody polyplexes displayed a size of 2000 nm and a zeta potential of approximately 20 mV. Furthermore, higher standard deviations of the PDI indicated greater size dispersity in these polyplexes. Previous studies have demonstrated that surface modifications, particularly involving protein characteristics and positioning, significantly influence particle size and charge. Additionally, high ionic strengths and elevated protein content can contribute to particle aggregation, potentially reducing the stability and applicability of the polyplexes in certain settings. (Kandil et al., 2019; Guerrini et al., 2018) In case of blending C14-PEI with the C14-PEI-adffibody, a formulation with acceptable properties was obtained when only 10 % protein-modified C14-PEI was used. Their particle size of around 370 nm and zeta potential of nearly 21 mV reflect that with a decreased amount of negatively charged affibody, the zeta potential is less affected, leading to acceptable colloidal stability.

3.8. Pre-functionalization: mRNA delivery with C14-PEI-affibody polyplexes

Polyplexes were prepared by blending 0 %, 10 %, and 30 % C14-PEI-affibody or PEI-affibody conjugates with C14-PEI. These polyplexes were then transfected with Cy5-labeled eGFP mRNA into A549, Hop62, and H358 cells to assess cellular internalization and expression (Figs. 7A and B). After 24 h, PEI-affibody conjugated polyplexes demonstrated a modest increase in cellular uptake with higher affibody content in A549 cells. However, this increase appeared to be more a result of differences in particle characteristics such as size and zeta potential rather than receptor-mediated internalization, as A549 cells have low Erbb3 receptor expression. Conversely, C14-PEI-affibody conjugates resulted in decreased uptake, which correlated with the density of C14-PEI-affibody. Furthermore, all formulations across the three cell lines showed generally reduced eGFP mRNA expression in the presence of affibody conjugates.

We confirmed that the expressed affibody can specifically bind to Erbb3, which fits the literature reports (Figs. 5A), (Schardt et al., 2017) and observed a trend in which PEI-affibody conjugates may increase retention in targeted cell populations (Figures S5A and S5C). Nonetheless, the performance of affibody-conjugated polyplexes varied with different formulations and conjugates. This variability may be due to several factors. First, as previously noted, an excess of antibodies can alter particle size, PDI, and zeta potential, impacting their behavior in biological systems. (Guerrini et al., 2018) Therefore, parameters need optimization for each blend ratio as they can vary significantly (Figs. 6A and 6B). Second, the position, density, and flexibility of antibodies on nanoparticles can significantly influence targeting efficiency. (Yong et al., 2020) The reaction between thiol and primary amine moieties from cysteine and lysine residues can lead to random antibody orientation, resulting in inefficient ligand packing and reduced

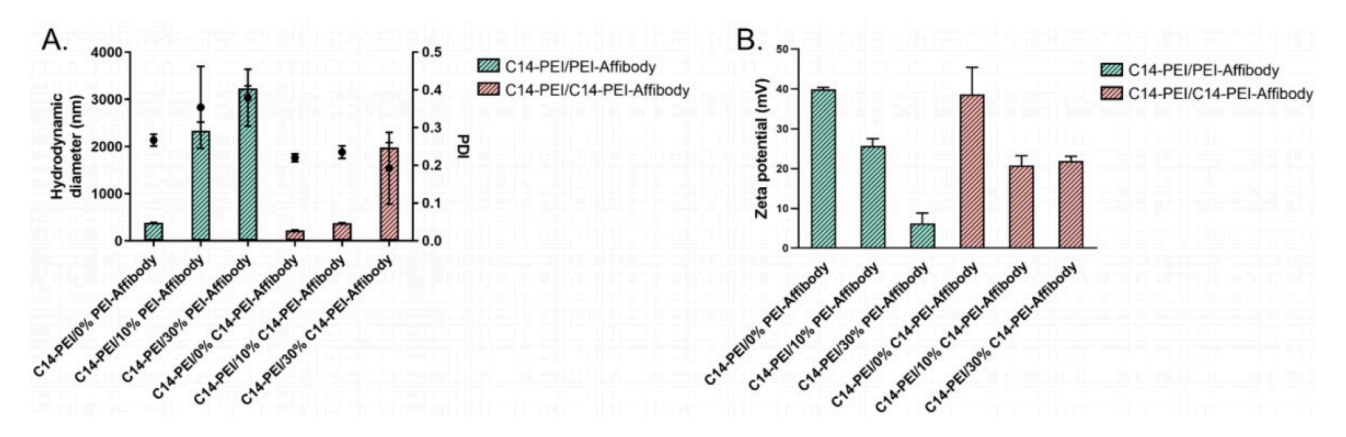


Fig. 6. Characterization of C14-PEI/PEI-affibody and C14-PEI/C14-PEI-affibody polyplexes. A) hydrodynamic diameter (bars) and PDI (dots) of polyplexes (n = 3); B) zeta potential of polyplexes (n = 3).

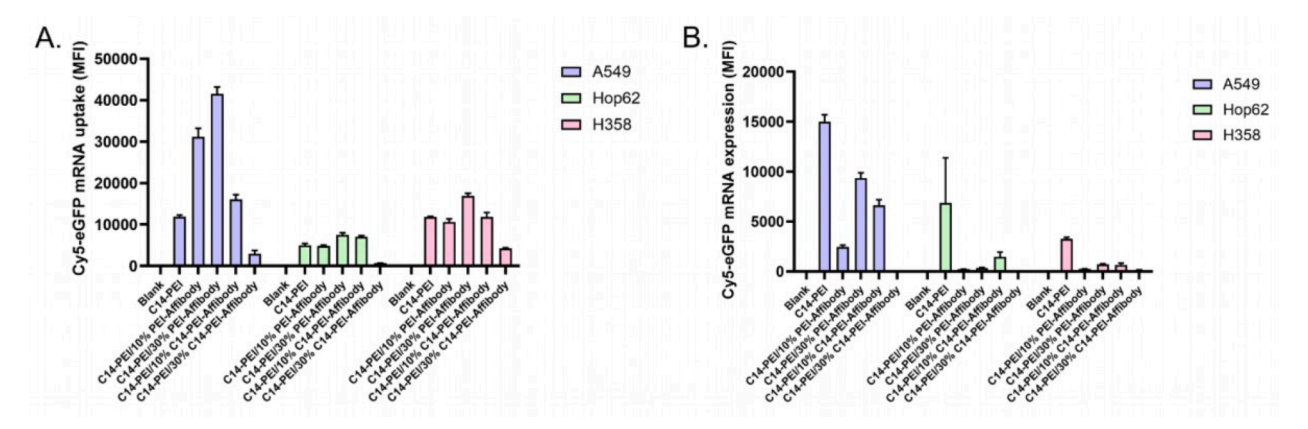


Fig. 7. Delivery of C14-PEI/PEI-affibody and C14-PEI/C14-PEI-affibody polyplexes in A549, Hop62, and H358 cells. A) Uptake of polyplexes measured by Flow Cytometry (n = 3); B) eGFP expression of polyplexes measured by Flow Cytometry (n = 3).

antigen-binding activity. (Polo et al., 2013) Thus, the conjugation method and choice of linkers are critical. Studies have shown that "click chemistry" offers high stereospecificity and yield with minimal by-products under mild conditions. (Jurgens et al., 2024; Lallana et al., 2012) Additionally, the route of cellular uptake can be affected by the type of targeting agent. While scavenger receptor-mediated endocytosis is common for nanoparticle uptake, some targeting ligands may facilitate receptor-specific uptake. (Valcourt et al., 2018) Our recent research highlighted that monovalent ligands often cannot compete with multivalent ones. (Jones et al., 2017) However, other studies suggest that for certain antibody-mediated endocytosis processes, such as transferrin clathrin-mediated internalization, size may be more crucial than multivalency due to the limited size of natural clathrin-coated pits. (Papademetriou et al., 2013; Hirst and Robinson, 1998) In the reported experiments, the surface charge seems to affect cellular uptake most importantly. However, to exclude the possibility of impaired affibody recognition by the receptor post-coupling, affinity tests were performed.

3.9. Post-functionalization: C14-PEI/PEI Azide polyplex preparation

In the pre-modification approach, during nanoparticle formation, the affibody may become embedded or oriented toward the nanoparticle core, potentially limiting its accessibility. Given the suboptimal results observed with pre-functionalized C14-PEI-affibody polyplexes—including undesirable particle size, surface charge, and reduced mRNA expression—a post-modification strategy was adopted to enable better control over affibody density and orientation. Click chemistry, known for its high stereospecificity and efficiency, offers a reliable approach to ligand conjugation under mild conditions with minimal byproduct formation. (Jurgens et al., 2024; Lallana et al., 2012)

As noted previously, the primary amine groups in C14-PEI are occupied by C14 alkyl chains, potentially reducing affibody modification efficiency. To overcome this limitation, C14-PEI was excluded from post-functionalization. Instead, low-molecular-weight PEI was selected, and azido groups were introduced using Azido-PEG4-NHS-ester, generating Azido-PEI for subsequent affibody conjugation via click chemistry. Blends of unmodified C14-PEI with 0 %, 10 %, or 30 % Azido-PEI were then prepared to achieve optimal particle characteristics prior to affibody functionalization, while varying the number of available azides in the formulation to optimize ligand density for subsequent modifications. In line with the particle assembly in the pre-modification approach, polymer blend solutions and mRNA were batch-mixed and incubated to facilitate self-assembly at different N/P ratios. Polyplexes prepared solely with unmodified C14-PEI exhibited the most heterogeneous size distribution, with particle sizes ranging from 84 nm to approximately 2900 nm at an N/P ratio of 7, indicating substantial aggregation (Fig. 8A). The zeta potential was slightly below 9 mV (Fig. 8B). Incorporating Azido-PEI into the formulation led to a slight increase in zeta potential except for C14/10 % PEI at N/P ratio 3, likely due to the additional positive charge of PEI, though it remained within a moderate range below 15 mV. Before affibody functionalization, all polyplexes containing PEI blends exhibited a favorable hydrodynamic diameter of less than 170 nm and PDIs of approximately 0.2 to 0.3, reflecting an acceptable size dispersity. These characteristics provided a suitable foundation for subsequent affibody modification, ensuring optimal conditions for post-functionalization.

3.10. Post-functionalization: Affibody conjugation via click chemistry

The affibody was modified with DBCO, incorporating a 12-unit PEG

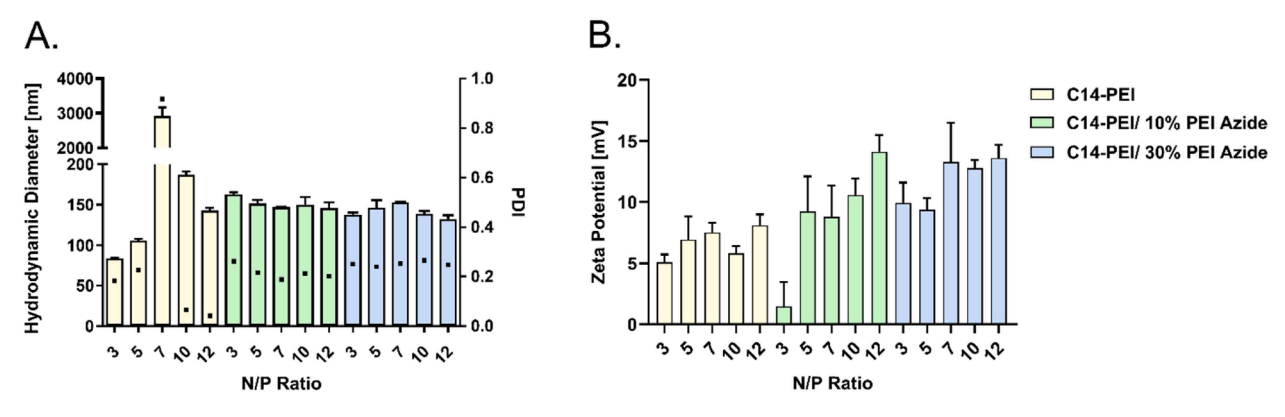


Fig. 8. Characterization of C14-PEI and C14-PEI/Azido-PEI polyplexes. A) hydrodynamic diameter (bars) and PDI (dots) of polyplexes (n = 3); B) zeta potential of polyplexes (n = 3).

spacer, consistent with the spacer length used in the pre-modification method. In the post-modification approach, the PEG spacer offers several advantages, including preventing adsorption to the cell surface by keeping targeting ligands exposed and accessible, potentially enhancing recognition and binding efficiency. Additionally, it may improve flexibility, facilitating receptor interactions. The purified DBCO-PEG12-Affibody was added to the polyplexes at a 1:10 (DBCO: Azides) ratio and incubated for 2 h to enable the strain-promoted azidealkyne click chemistry reaction, forming a stable triazole bond between the azide-tagged polyplexes and the DBCO-functionalized affibody. Following conjugation, an increase in hydrodynamic diameter was observed across all formulations. For C14/10 % PEI-Affibody polyplexes, particle sizes ranged from approximately 215 to 420 nm, with PDIs generally remaining below 0.4 (Fig. 9A). In contrast, for C14/30 % PEI-Affibody polyplexes, both size and PDI increased to around 300 nm and 0.3-0.4, respectively, for all N/P ratios except N/P 12, where the near-neutral zeta potential led to aggregation and a highly polydisperse distribution (Fig. 9B). Compared to non-conjugated or prefunctionalized polyplexes, most post-modified formulations exhibited a lower zeta potential, indicating the presence of the negatively charged affibody. Notably, the post-modification approach resulted in significantly smaller polyplexes than the pre-conjugation method, demonstrating improved control over particle size.

3.11. Post-functionalization: mRNA delivery with C14-PEI-afiibody polyplexes

Subsequently, cellular uptake (Figs. 10A.1–3) and transfection efficiency (Figs. 10B1–3) of post-modified polyplexes encapsulating AF647-labeled eGFP mRNA were investigated, with varying amounts of PEI-Affibody (0 %, 10 %, or 30 %) and different N/P ratios (7, 10, and 12). The experiments were conducted in A549, H358, and Hop62 cells, with non-conjugated polyplexes serving as controls to assess the impact of ligand-mediated targeting. Lipofectamine was used as a positive control for transfection efficiency.

Overall, high cellular uptake and increased eGFP expression induced by C14-PEI polyplexes at N/P ratio 7 in A549 and H358 cells was observed. This effect is likely attributable to the aggregation of the particles, which may facilitate cellular interaction and internalization. Interestingly, in A549 cells, a clear correlation was observed, where post-modified affibody polyplexes exhibited significantly higher uptake and transfection efficiency compared to their non-conjugated counterparts. Despite the fact that A549 cells express lower levels of Erbb3 receptors than H358 and Hop62, the enhanced uptake and expression could still be attributed to receptor-mediated endocytosis as the presentation of multiple ligands on the polyplex surface – unlike single ligands - can compensate for a lower receptor density, which in turn enhances internalization. (Chen et al., 2022)

In contrast, the uptake pattern in H358 and Hop62 cells did not

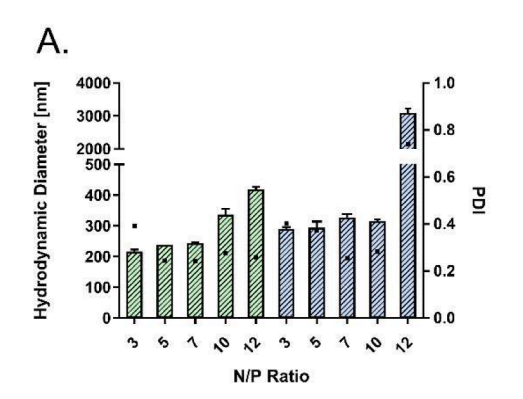
reveal a clear trend, despite their inherently higher Erbb3 receptor expression levels. However, in both cell lines, the highest uptake was observed for affibody conjugated polyplexes with lower ligand densities at N/P 10 in H358 and N/P 7 in Hop62, respectively. The absence of a consistent trend suggests that uptake in these cells is not solely driven by receptor-mediated endocytosis but may also be influenced by other factors. Differences in particle size, zeta potential, or cellular internalization mechanisms could contribute to the observed variability. Additionally, variations in endocytic pathways across different cell lines might affect the efficiency of polyplex internalization, further complicating the interpretation of the data. For C14/30 % PEI-Affibody polyplexes, no significant differences were observed between the targeted and non-conjugated particles. This indicates that non-conjugated polyplexes may already possess physicochemical properties that enhance their non-specific uptake, thereby masking any receptor-specific targeting effects. Factors such as a more positive zeta potential or smaller particle size may facilitate interactions with the negatively charged cell membrane, leading to increased internalization independent of receptor engagement for the non-targeted polyplexes.

Despite the inconsistent uptake trends in H358 and Hop62 cells, eGFP expression data revealed a clear advantage of affibodyfunctionalized polyplexes compared to non-conjugates nanoparticles across all three cell lines. In Hop62 cells, affibody-polyplexes—particularly C14/10 % PEI-Affibody polyplexes at N/P ratios of 7 and 12—demonstrated superior transfection efficiency compared to non-targeted nanoparticles and even Lipofectamine, indicating that ligand-mediated targeting enhances gene delivery. This implies that effective delivery and intracellular processing of the encapsulated mRNA may play a more significant role in transfection success than uptake alone. A particularly intriguing finding was that formulations with 10 % PEI-Affibody (i.e., also lower Affibody density) exhibited stronger uptake and transfection effects compared to those with 30 % PEI-Affibody functionalization. Given that these formulations displayed similar particle sizes and zeta potentials, the observed differences are likely attributable to the ligand density on the polyplex surface. Previous studies have demonstrated that excessively high ligand densities can paradoxically reduce overall binding affinity, potentially due to steric hindrance. (Chen et al., 2022)

This underscores the importance of optimizing ligand presentation to balance efficient receptor interaction and internalization.

4. Conclusion & prospect

mRNA-based polyplexes offer several advantages, including transient expression with controlled, time-limited therapeutic effects, avoidance of genomic integration that preserves the integrity of the host genome, and reduced immunogenicity compared to viral vectors. (Kowalski et al., 2019; Qin et al., 2022; Li et al., 2023) These benefits highlight the safety and increasing interest in mRNA-based polyplex



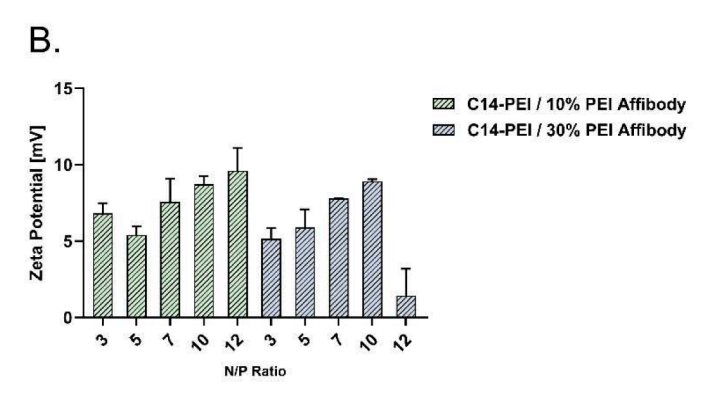


Fig. 9. Characterization of C14-PEI and C14-PEI/PEI-Affibody polyplexes. A) hydrodynamic diameter (bars) and PDI (dots) of polyplexes (n = 3); **B)** zeta potential of polyplexes (n = 3).

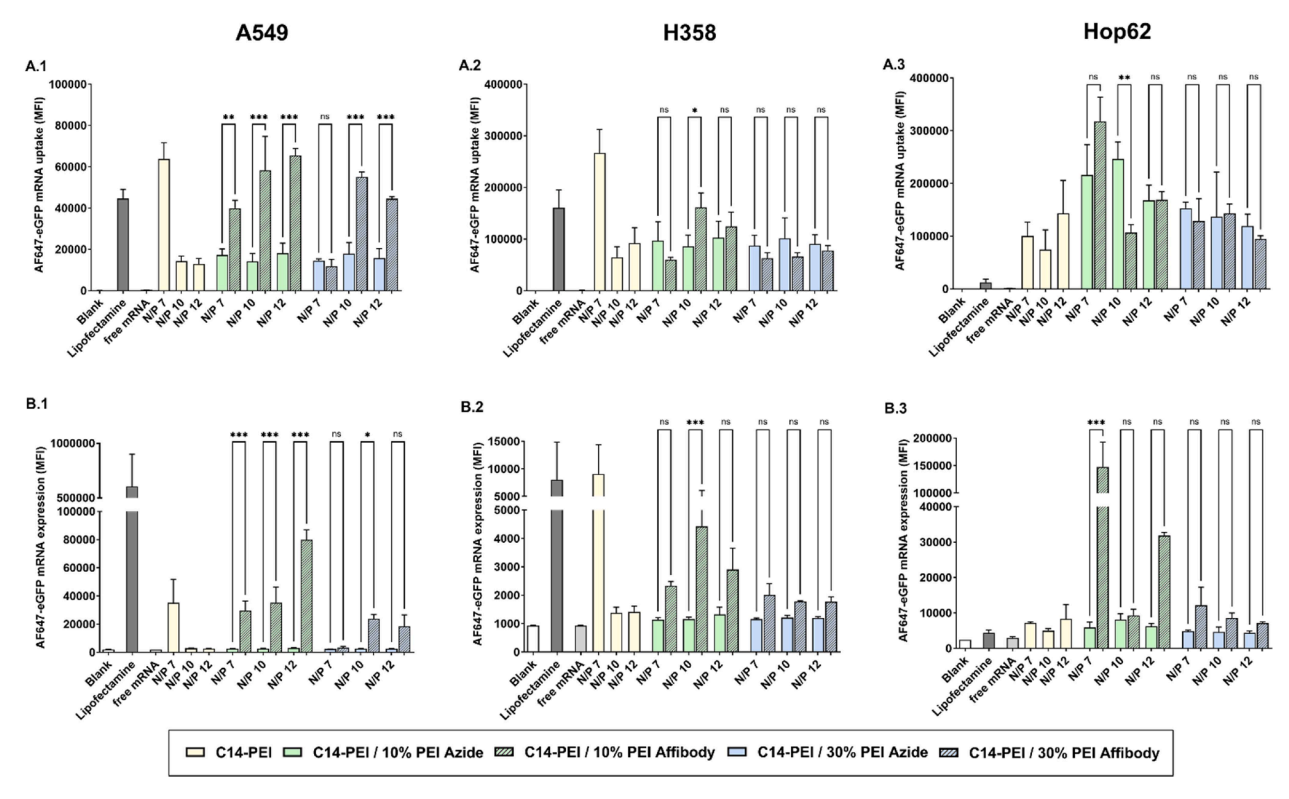


Fig. 10. Delivery of C14-PEI/PEI-azides and C14-PEI/PEI-affibody polyplexes with different N/P ratios in A549, Hop62, and H358 cells. A.1–3) Uptake of polyplexes measured by Flow Cytometry (n = 3); one-way ANOVA, *p < 0.05 **p < 0.01, ***p < 0.001, and ns = nonsignificant.

delivery. Antibody conjugation in the engineering of polyplexes offers the dual benefit of prolonging cell surface binding, thereby enhancing polyplex uptake, while also ensuring selective binding to target cells. This approach provides a safe, biocompatible, and targeted method for delivering mRNA to specific cells and tissues. (Luks et al., 2022) In this study, we used an engineered affibody as a proof-of-concept targeting ligand due to its well-documented characteristics and the ability to target the Erbb3 receptor, which is relevant for lung cancer delivery. After confirming Erbb3 overexpression in KRAS mutant lung cancer cells and the binding between affibody and Erbb3, polyplexes were successfully prepared using two conjugation approaches: pre-conjugation of the polymer before polyplex formation and post-conjugation by spiking the affibody after polyplex assembly. Although spectral shift measurements confirmed the binding affinity between the HER3 receptor and our affibody conjugates, this interaction did not translate into functional efficacy after formulation of the polyplexes. The pre-functionalized targeted nanoparticles failed to enhance mRNA expression, and eGFP expression in the affibody-modified polyplexes showed no correlation with Erbb3 expression levels across the tested cell lines. This suggests that the pre-functionalized C14-PEI-affibody may not have been optimally oriented or accessible for effective receptor interaction. In contrast, the results of post-modified affibody-functionalized nanoparticles show evidence for receptor-mediated targeting, as seen in A549 cells, where uptake and transfection efficiency increased despite low Erbb3 expression. The superior performance of affibody-polyplexes over Lipofectamine in Hop62 cells further supports ligand-mediated targeting. Additionally, the optimal ligand density (10 % PEI-Affibody) enhanced uptake and expression, highlighting the importance of controlled ligand presentation. While non-specific uptake may contribute, the clear transfection benefits of affibody conjugation suggest a functional targeting effect.

We hypothesize that the post-modification approach enhances affibody orientation toward the nanoparticle surface, whereas in the preconjugation approach, the affibody may become partially embedded within the nanoparticle core, limiting its accessibility for receptor interaction. However, further investigation is required to confirm this effect. Our study provides insights into the targeting capabilities of affibody-conjugated polyplexes. We observed that particle size, PDI, surface charge, uptake, and expression were influenced by changes in polyplex formulation, conjugation strategy, and affibody density. We demonstrated that by adjusting the formulation and affibody density, we were able to modify binding behaviors. Further research is needed to optimize nanoparticle characteristics and delivery efficiency by refining formulation and conjugation methods. Additionally, evaluating the most effective transport pathways for targeted polyplex delivery is essential.

Overall, our affibody-conjugated polyplexes have shown promise for targeting lung cancer cells, suggesting that inhalation via nebulization or dry powder inhalers could be an effective method for delivering these polyplexes directly to the lungs (Zimmermann et al., 2022). Inhalation offers a highly targeted route of administration, which could be particularly beneficial for treating lung diseases. By delivering the polyplexes directly to the respiratory system, this approach minimizes systemic exposure while enhancing local therapeutic effects (Jin et al., 2023). For example, Cabibbo and colleagues recently developed an inhalable formulation using lipid-polymer hybrid systems for pulmonary delivery of siRNA (Cabibbo et al., 2025). Their formulation demonstrated high cellular uptake and about 50 % gene silencing efficiency in human lung cancer cells expressing GFP. However, while targeted polyplexes are designed to bind primarily to specific cells, there is still the potential for off-target uptake, albeit at lower levels. This unintended uptake could lead to cellular stress, inflammation, or cytotoxicity, particularly at high concentrations or if the polyplexes are not fully optimized for biocompatibility (Ezhilarasan et al., 2022). The inhalation route could reduce these risks by ensuring localized delivery to lung tissues, limiting systemic exposure and improving therapeutic outcomes (Keil et al., 2021). Additionally, when paired with targeted cargo, such as Cas9 mRNA and sgRNA for gene therapy (Chen et al., 2025), side effects could be minimized due to the specificity of the ligands and nucleic acid sequences. Future studies will focus on a more detailed evaluation of the toxicity profiles of these polyplexes, including potential effects on non-target cells and tissues, using in vivo models. Further optimization of the polymer composition, surface charge, and particle size will also be key to reducing non-specific uptake and enhancing biocompatibility (Chen et al., 2025). In conclusion, our findings validate the strategy of affibody conjugation with polyplexes, laying the groundwork for future studies and providing a promising platform for understanding ligand conjugation in the targeted delivery of mRNA.

CRediT authorship contribution statement

Siyu Chen: Writing – original draft, Visualization, Methodology, Investigation, Formal analysis, Data curation. Anny Nguyen: Formal analysis, Investigation, Methodology, Visualization, Writing - original draft. Joschka T. Müller: Investigation, Methodology, Visualization, Writing – review & editing. Müge Molbay: Investigation, Methodology, Writing - review & editing. Aditi Mehta: Writing - review & editing, Methodology, Investigation, Conceptualization. Sahana Sheshachala: Writing - review & editing, Methodology, Investigation, Formal analysis. Kemal Baskaya: Methodology, Investigation. Nathan Adams: Writing – review & editing, Resources. Simone Pinto Carneiro: Writing - review & editing, Supervision, Methodology, Conceptualization. Olivia M. Merkel: Writing - review & editing, Supervision, Resources, administration, Methodology, Funding acquisition, Project Conceptualization.

Acknowledgment

The authors thank Prof. Georgios Stathopoulos for providing the Hop62 and H358M cells. Siyu Chen acknowledges the financial support from the China Scholarship Council (CSC). Simone Carneiro thanks the financial support from the Alexander von Humboldt Foundation and the Center of Nanoscience (CeNS) Munich. Sahana Sheshachala would like to acknowledge Tobiaz Pirzer and Andreas Langer (Nanotemper Technologies GmBH) for expert discussions. This research was partially funded by ERC-2014-StG-637830 to Olivia Merkel and by the BMBF within the framework of the Cluster4Future program (Cluster for Nucleic Acid Therapeutics Munich, CNATM) (Project ID: 03ZU1201AA).

Supplementary materials

Supplementary material associated with this article can be found, in the online version, at doi:10.1016/j.ejps.2025.107090.

Data availability

Data will be made available on request.

References

- Abramson, J., et al., 2024. Accurate structure prediction of biomolecular interactions with AlphaFold 3. Nature 630, 493–500. https://doi.org/10.1038/s41586-024-07487-w.
- Barr, T., Ma, S., Li, Z., Yu, J., 2024. Recent advances and remaining challenges in lung cancer therapy. Chin. Med. J. (Engl) 137, 533–546. https://doi.org/10.1097/
- Beji, A., Horst, D., Engel, J., Kirchner, T., Ullrich, A., 2012. Toward the prognostic significance and therapeutic potential of HER3 receptor tyrosine kinase in human colon cancer. Clin. Cancer Res. 18, 956–968. https://doi.org/10.1158/1078-0432. CCR_11_1186
- Bray, F., et al., 2024. Global cancer statistics 2022: GLOBOCAN estimates of incidence and mortality worldwide for 36 cancers in 185 countries. CA Cancer J. Clin. 74, 229–263. https://doi.org/10.3322/caac.21834.
- Cabibbo, M., et al., 2025. Diving into RNAi therapy: an inhalable formulation based on lipid-polymer hybrid systems for pulmonary delivery of siRNA. Biomacromolecules. 26, 163–177. https://doi.org/10.1021/acs.biomac.4c00387.
- Chen, C., Zhou, Y., Chen, C., Zhu, S., Yan, X., 2022. Quantification of available ligand density on the surface of targeted liposomal nanomedicines at the single-particle level. ACS. Nano 16, 6886–6897. https://doi.org/10.1021/acsnano.2c02084.

- Chen, S., Triki, M., Pinto Carneiro, S., Merkel, O.M., 2025a. A novel micelleplex for tumour-targeted delivery of CRISPR-Cas9 against KRAS-mutated lung cancer. Nanoscale. https://doi.org/10.1039/D4NR03471F.
- Chen, S., Pinto Carneiro, S., Merkel, O.M., 2025b. Anionic polymer coating for enhanced delivery of Cas9 mRNA and sgRNA nanoplexes. Biomater. Sci. 13, 659–676. https:// doi.org/10.1039/d4bm01290a.
- Cho, H.S., Leahy, D.J., 2002. Structure of the extracellular region of HER3 reveals an interdomain tether. Science (1979) 297, 1330–1333. https://doi.org/10.1126/ science.1074611.
- Coldren, C.D., et al., 2006. Baseline gene expression predicts sensitivity to gefitinib in non-small cell lung cancer cell lines. Mol. Cancer Res. 4, 521–528. https://doi.org/ 10.1158/1541-7786 MCR-06-0095
- D'Souza A., A., Shegokar, R., 2016. Polyethylene glycol (PEG): a versatile polymer for pharmaceutical applications. Expert. Opin. Drug Deliv. 13, 1257–1275. https://doi. org/10.1080/17425247.2016.1182485.
- de Sousa, V.M.L., Carvalho, L., 2018. Heterogeneity in lung cancer. Pathobiology 85, 96–107. https://doi.org/10.1159/000487440.
- Ezhilarasan, D., Lakshmi, T., Mallineni, S.K., 2022. Nano-based targeted drug delivery for lung cancer: therapeutic avenues and challenges. Nanomedicine (Lond) 17, 1855–1869. https://doi.org/10.2217/nnm-2021-0364.
- Froger, A., Hall, J.E., 2007. Transformation of plasmid DNA into E. coli using the heat shock method. J. Vis. Exp. 253. https://doi.org/10.3791/253.
- Gabold, B., et al., 2023. Transferrin-modified chitosan nanoparticles for targeted nose-to-brain delivery of proteins. Drug Deliv. Transl. Res. 13, 822–838. https://doi.org/ 10.1007/s13346-022-01245-z
- Goldman, M.J., et al., 2020. Visualizing and interpreting cancer genomics data via the Xena platform. Nat. Biotechnol. 38, 675–678. https://doi.org/10.1038/s41587-020-0546-8
- Guerrini, L., Alvarez-Puebla, R.A., Pazos-Perez, N., 2018. Surface modifications of nanoparticles for stability in biological fluids. Materials. (Basel) 11. https://doi.org/ 10.3390/ma11071154.
- He, Y., et al., 2022. Liposomes and liposome-like nanoparticles: from anti-fungal infection to the COVID-19 pandemic treatment. Asian J. Pharm. Sci. 17, 817–837. https://doi.org/10.1016/j.ajps.2022.11.002.
- Helmschrodt, C., et al., 2017. Polyethylenimine nanoparticle-mediated siRNA delivery to reduce alpha-synuclein expression in a model of Parkinson's Disease. Mol. Ther. Nucleic. Acids. 9, 57–68. https://doi.org/10.1016/j.omtn.2017.08.013.
- Hirst, J., Robinson, M.S.Clathrin, adaptors, 1998. Biochim. Biophys. Acta 1404, 173–193. https://doi.org/10.1016/s0167-4889(98)00056-1.
- Jang, S.C., et al., 2013. Bioinspired exosome-mimetic nanovesicles for targeted delivery of chemotherapeutics to malignant tumors. ACS. Nano 7, 7698–7710. https://doi. org/10.1021/nn402232g.
- Jay, S.M., et al., 2011. Engineered bivalent ligands to bias ErbB receptor-mediated signaling and phenotypes. J. Biol. Chem. 286, 27729–27740. https://doi.org/ 10.1074/jbc.M111.221093.
- Jin, Z., et al., 2023. Harnessing inhaled nanoparticles to overcome the pulmonary barrier for respiratory disease therapy. Adv. Drug Deliv. Rev. 202, 115111. https://doi.org/ 10.1016/j.addr.2023.115111.
- Jin, Y., et al., 2024. Role of hydrophobic modification in spermine-based poly(β-amino ester)s for siRNA delivery and their spray-dried powders for inhalation and improved storage. Biomacromolecules. https://doi.org/10.1021/acs.biomac.4c00283.
- Johnston, B.M., Grodzinsky, A.J., Hammond, P.T., 2023. Charge shielding effects of PEG bound to NH(2)-terminated PAMAM dendrimers - an experimental approach. Soft. Matter. 19, 3033–3046. https://doi.org/10.1039/d2sm01698b.
- Jones, S.K., Sarkar, A., Feldmann, D.P., Hoffmann, P., Merkel, O.M., 2017. Revisiting the value of competition assays in folate receptor-mediated drug delivery. Biomaterials 138, 35–45. https://doi.org/10.1016/j.biomaterials.2017.05.034.
- Jurgens, D.C., Muller, J.T., Nguyen, A., Merkel, O.M., 2024. Tailoring lipid nanoparticles for T-cell targeting in allergic asthma: insights into efficacy and specificity. Eur. J. Pharm. Biopharm. 198, 114242. https://doi.org/10.1016/j.ejpb.2024.114242.
- Kandil, R., et al., 2019. Coming in and finding out: blending receptor-targeted delivery and efficient endosomal escape in a novel bio-responsive siRNA delivery system for gene knockdown in pulmonary T cells. Adv. Ther. (Weinh) 2. https://doi.org/ 10.1002/adtp.201900047.
- Kandil, R., Xie, Y., Mehta, A., Merkel, O., 2020. A method for targeted nonviral siRNA delivery in cancer and inflammatory diseases. Methods Mol. Biol. 2059, 155–166. https://doi.org/10.1007/978-1-4939-9798-5_7.
- Keil, T.W., et al., 2021. Impact of crystalline and amorphous matrices on successful spray drying of siRNA polyplexes for inhalation of nano-in-microparticles. Adv. Ther. (Weinh) 4. https://doi.org/10.1002/adtp.202100073.
- Kowalski, P.S., Rudra, A., Miao, L., Anderson, D.G., 2019. Delivering the Messenger: advances in technologies for therapeutic mRNA delivery. Mol. Ther. 27, 710–728. https://doi.org/10.1016/j.ymthe.2019.02.012.
- Kronqvist, N., et al., 2011. Combining phage and staphylococcal surface display for generation of ErbB3-specific affibody molecules. Protein Eng. Des. Sel. 24, 385–396. https://doi.org/10.1093/protein/gzq118.
- Kumagai, T., et al., 2018. HER3 expression is enhanced during progression of lung adenocarcinoma without EGFR mutation from stage 0 to IA1. Thorac. Cancer 9, 466–471. https://doi.org/10.1111/1759-7714.12609.
- Lallana, E., Sousa-Herves, A., Fernandez-Trillo, F., Riguera, R., Fernandez-Megia, E., 2012. Click chemistry for drug delivery nanosystems. Pharm. Res. 29, 1–34. https://doi.org/10.1007/s11095-011-0568-5.
- Langer, A., et al., 2022. A New Spectral Shift-Based Method to Characterize Molecular Interactions. Assay Drug Dev. Technol. 20, 83–94. https://doi.org/10.1089/ adt.2021.133.

- Lee, K., et al., 2017. Nanoparticle delivery of Cas9 ribonucleoprotein and donor DNA in vivo induces homology-directed DNA repair. Nat. Biomed. Eng. 1, 889–901. https:// doi.org/10.1038/s41551-017-0137-2.
- Leiter, A., Veluswamy, R.R., Wisnivesky, J.P., 2023. The global burden of lung cancer: current status and future trends. Nat. Rev. Clin. Oncol. 20, 624–639. https://doi.org/ 10.1038/s41571-023-00798-3.
- Li, D.F., et al., 2023. Nanomaterials for mRNA-based therapeutics: challenges and opportunities. Bioeng. Transl. Med. 8, e10492. https://doi.org/10.1002/ btm2.10492.
- Li, W., et al., 2024. mRNA-lipid nanoparticle-mediated restoration of PTPN14 exhibits antitumor effects by overcoming anoikis resistance in triple-negative breast cancer. Adv. Sci. (Weinh) 11, e2309988. https://doi.org/10.1002/advs.202309988.
- Lipton, A., et al., 2013. HER3, p95HER2, and HER2 protein expression levels define multiple subtypes of HER2-positive metastatic breast cancer. Breast. Cancer Res. Treat. 141, 43–53. https://doi.org/10.1007/s10549-013-2665-0.
- Liu, Y., et al., 2023. Nanoparticles advanced from preclinical studies to clinical trials for lung cancer therapy. Cancer Nanotechnol. 14, 28. https://doi.org/10.1186/s12645-023.00174 x
- Lokras, A.G., Bobak, T.R., Baghel, S.S., Sebastiani, F., Foged, C., 2024. Advances in the design and delivery of RNA vaccines for infectious diseases. Adv. Drug Deliv. Rev., 115419 https://doi.org/10.1016/j.addr.2024.115419.
- Luks, V.L., et al., 2022. Surface conjugation of antibodies improves nanoparticle uptake in bronchial epithelial cells. PLoS. One 17, e0266218. https://doi.org/10.1371/ journal.pone.0266218.
- Mishra, R., Patel, H., Alanazi, S., Yuan, L., Garrett, J.T., 2018. HER3 signaling and targeted therapy in cancer. Oncol. Rev. 12, 355. https://doi.org/10.4081/ oncol.2018.355
- Papademetriou, J., et al., 2013. Comparative binding, endocytosis, and biodistribution of antibodies and antibody-coated carriers for targeted delivery of lysosomal enzymes to ICAM-1 versus transferrin receptor. J. Inherit. Metab. Dis. 36, 467–477. https:// doi.org/10.1007/s10545-012-9534-6.
- Polo, E., et al., 2013. Tips for the functionalization of nanoparticles with antibodies. Methods Mol. Biol. 1051, 149–163. https://doi.org/10.1007/978-1-62703-550-7
- Qian, G., et al., 2015. Heregulin and HER3 are prognostic biomarkers in oropharyngeal squamous cell carcinoma. Cancer 121, 3600–3611. https://doi.org/10.1002/
- Qin, S., et al., 2022. mRNA-based therapeutics: powerful and versatile tools to combat diseases. Signal. Transduct. Target. Ther. 7, 166. https://doi.org/10.1038/s41392-022-01007-w.

- Ramakrishna, S., et al., 2014. Gene disruption by cell-penetrating peptide-mediated delivery of Cas9 protein and guide RNA. Genome Res. 24, 1020–1027. https://doi. org/10.1101/gr.171264.113.
- Ryan, A., et al., 2021. Pharmaceutical design of a delivery system for the bacteriocin lacticin 3147. Drug Deliv. Transl. Res. 11, 1735–1751. https://doi.org/10.1007/ s13346-021-00984-9.
- Schardt, J.S., et al., 2017. Engineered multivalency enhances affibody-based HER3 inhibition and downregulation in cancer cells. Mol. Pharm. 14, 1047–1056. https://doi.org/10.1021/acs.molpharmaceut.6b00919.
- Sithanandam, G., Anderson, L.M., 2008. The ERBB3 receptor in cancer and cancer gene therapy. Cancer Gene Ther. 15, 413–448. https://doi.org/10.1038/cgt.2008.15.
- Stahl, S., et al., 2017. Affibody molecules in biotechnological and medical applications. Trends Biotechnol. 35, 691–712. https://doi.org/10.1016/j.tibtech.2017.04.007.
- Tanner, B., et al., 2006. ErbB-3 predicts survival in ovarian cancer. J. Clin. Oncol. 24, 4317–4323. https://doi.org/10.1200/JCO.2005.04.8397.
- Valcourt, D.M., et al., 2018. Advances in targeted nanotherapeutics: from bioconjugation to biomimicry. Nano Res. 11, 4999–5016. https://doi.org/10.1007/s12274-018-2083-z.
- Wadajkar, A.S., et al., 2017. Tumor-targeted nanotherapeutics: overcoming treatment barriers for glioblastoma. Wiley. Interdiscip. Rev. Nanomed. Nanobiotechnol. 9. https://doi.org/10.1002/wnan.1439.
- Wang, Z., et al., 2017. Active targeting theranostic iron oxide nanoparticles for MRI and magnetic resonance-guided focused ultrasound ablation of lung cancer. Biomaterials 127, 25–35. https://doi.org/10.1016/j.biomaterials.2017.02.037.
- Witta, S.E., et al., 2009. ErbB-3 expression is associated with E-cadherin and their coexpression restores response to gefitinib in non-small-cell lung cancer (NSCLC). Ann. Oncol. 20, 689–695. https://doi.org/10.1093/annonc/mdn703.
- Woodman, C., Vundu, G., George, A., Wilson, C.M., 2021. Applications and strategies in nanodiagnosis and nanotherapy in lung cancer. Semin. Cancer Biol. 69, 349–364. https://doi.org/10.1016/j.semcancer.2020.02.009.
- Wu, J., 2021. The enhanced permeability and retention (EPR) effect: the significance of the concept and methods to enhance its application. J. Pers. Med. 11. https://doi. org/10.3390/jpm11080771.
- Yong, K.W., Yuen, D., Chen, M.Z., Johnston, A.P.R., 2020. Engineering the orientation, density, and flexibility of single-domain antibodies on nanoparticles to improve cell targeting. ACS. Appl. Mater. Interfaces. 12, 5593–5600. https://doi.org/10.1021/acsami/9h20993
- Zimmermann, C.M., et al., 2022. Spray drying siRNA-lipid nanoparticles for dry powder pulmonary delivery. J. Control Release 351, 137–150. https://doi.org/10.1016/j. jconrel.2022.09.021.